

# MD-Splatting: Learning Metric Deformation from 4D Gaussians in Highly Deformable Scenes

Bardienus P. Duisterhof  
Carnegie Mellon University  
bduister@cmu.edu

Zhao Mandi  
Stanford University  
mandi@stanford.edu

Yunchao Yao  
Carnegie Mellon University  
yunchao@andrew.cmu.edu

Jia-Wei Liu  
National University of Singapore  
jiawei.liu@u.nus.edu

Mike Zheng Shou  
National University of Singapore  
mike.zheng.shou@gmail.com

Shuran Song  
Stanford University  
shuran@stanford.edu

Jeffrey Ichnowski  
Carnegie Mellon University  
jeffi@cmu.edu

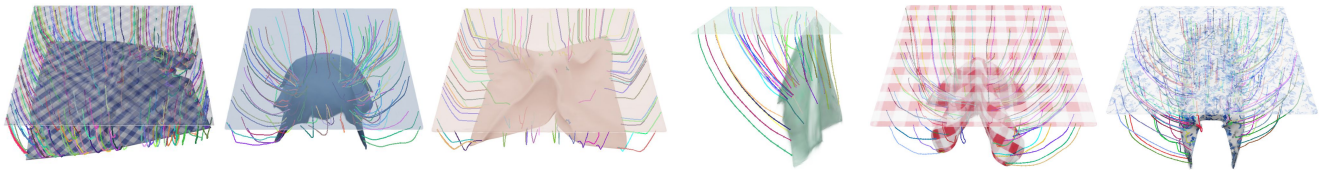


Figure 1. We propose MD-Splatting, a method that improves state-of-the-art methods for simultaneous dynamic novel view synthesis and accurate 3D point tracking in highly deformable scenes. This figure shows the rendering and tracking of MD-Splatting in the six dynamic Blender [11] scenes used for evaluation. We will refer to the scenes in this Figure as Scenes 1, 2, 3, 4, 5 and 6 ordered from left to right.

## Abstract

Accurate 3D tracking in highly deformable scenes with occlusions and shadows can facilitate new applications in robotics, augmented reality, and generative AI. However, tracking under these conditions is extremely challenging due to the ambiguity that arises with large deformations, shadows, and occlusions. We introduce MD-Splatting, an approach for simultaneous 3D tracking and novel view synthesis, using video captures of a dynamic scene from various camera poses. MD-Splatting builds on recent advances in Gaussian splatting, a method that learns the properties of a large number of Gaussians for state-of-the-art and fast novel view synthesis. MD-Splatting learns a deformation function to project a set of Gaussians with non-metric, thus canonical, properties into metric space. The deformation function uses a neural-voxel encoding and a multilayer perceptron (MLP) to infer Gaussian position, rotation, and a shadow scalar. We enforce physics-inspired regularization terms based on local rigidity, conservation of momentum, and isometry, which leads to trajectories with smaller trajectory errors. MD-Splatting achieves high-quality 3D tracking on highly deformable scenes with shadows and

occlusions. Compared to state-of-the-art, we improve 3D tracking by an average of 23.9 %, while simultaneously achieving high-quality novel view synthesis. With sufficient texture such as in scene 6, MD-Splatting achieves a median tracking error of 3.39 mm on a cloth of  $1 \times 1$  meters in size. Project Website: <https://md-splatting.github.io>

## 1. Introduction

Three-dimensional tracking of clothing, towels, and similarly highly deformable objects as they drop, deform, and drape can facilitate new applications and improve the capabilities of existing applications. Generative AI and augmented reality applications can benefit from novel view synthesis for training, interaction, and scene editing [21]. Robots can benefit from tracking task-relevant geometries to dexterously manipulate deformable objects [8, 46, 47] and use novel-view synthesis to augment learning [20]. Simulation methods can improve fidelity using *real2sim* and related approaches that leverage real-world tracking data for parameter and method tuning [28]. However, tracking mov-

ing and morphing points poses many non-trivial challenges: points change color as they pass through shadows, occlusions interfere with the continuous visibility of points, and internal and external forces, such as material tension and air currents, cause points to move unpredictably.

Recent work demonstrated Gaussian splatting [25] can yield state-of-the-art novel view synthesis and rendering speeds exceeding 100 fps. 3D Gaussian Splatting fits the properties of a set of Gaussians, their color, position, and covariance matrix, using a fast differentiable rasterizer. An extension of 3D Gaussian splatting [33] showed dynamic scenes can be modeled by explicitly optimizing the properties of Gaussians over time, including the metric deformations. Metric deformations are the changes in the position of Gaussians in the world frame between two adjacent timesteps. Metric deformations across many timesteps yields 3D tracking of Gaussians, contrary to related work [42] with deformations available only in a canonical frame.

Explicitly optimizing the Gaussian pose as in Dynamic 3D Gaussians [33], the most relevant baseline to MD-Splatting, results in degraded performance with large deformations and shadows. Training time also scales linearly with the number of timesteps provided for each camera, meaning longer sequences take proportionally longer to train.

We propose MD-Splatting, a method that uses time-synchronized image frames from a calibrated multi-camera setup to track 3D geometries of deformable objects as they move through shadows and occlusions. MD-Splatting learns the canonical state of a set of Gaussians and a deformation function that maps the Gaussians into metric space. This enables tracking by recovering metric deformations, and novel-view rendering (through splatting) using a fast differentiable rasterizer.

We evaluate MD-Splatting in six photo-realistic synthetic scenes of varying difficulty. The scenes contain large deformations, shadows, and occlusions (see Figure 1 for visualization of the scenes and tracking trajectories by MD-Splatting). Empirical results show that MD-Splatting infers 16.7 % more accurate 3D tracking results compared to previous state-of-the-art [33], and achieves high-quality novel-view reconstruction results with an average PSNR of 39.1. In a scene with cameras at 1 m radius from the origin (i.e. Scene 6), MD-Splatting can track cloth deformation with as low as 3.39 mm median tracking error. To the best of our knowledge, MD-Splatting is the first approach for 3D tracking and view synthesis using canonical Gaussian splats.

In summary, we contribute:

- The first approach that learns continuous metric deformations from a canonical space of Gaussians.
- Experiments that suggest state-of-the-art performance in simultaneous 3D metric tracking and novel view synthe-

sis. MD-Splatting improves tracking accuracy by an average of 16.7 % while achieving competitive view reconstruction.

- A set of six synthetic scenes with large deformations, strong shadows, and occlusions. The scenes will be shared with the community.

## 2. Related Work

MD-Splatting builds on prior work in novel view synthesis in dynamic scenes to enable simultaneous 3D tracking and novel view synthesis. We discuss prior works in novel view synthesis in static and dynamic scenes, as well as methods for point tracking.

### 2.1. Neural Rendering for Novel View Synthesis

MD-Splatting builds on prior work in novel view synthesis, and uses photometric consistency as a signal to achieve 3D tracking. A popular novel view synthesis approach is NeRF [34], which uses neural networks to learn scene representations that are capable of photo-realistic novel view reconstruction. The learned networks render a 3D point by outputting its RGB radiance and density when viewed from an arbitrary camera view. NeRF then renders pixels using existing volume rendering techniques. Subsequent works improve NeRF along several axes: one is to speed up training and inference time via novel representations and system optimizations [19, 31, 32, 35, 36, 36, 44, 50, 68], or depth supervision [1, 12, 37, 49, 63]. Other works extend NeRF to more challenging conditions, such as sparser camera views [10, 39, 54, 69], fewer extrinsic camera calibrations [9, 24, 29, 66], transparent objects [23, 26] and reflective surfaces [57].

Particle-based methods use a more explicit representation than typical NeRF-based approaches. MD-Splatting builds on 3D Gaussian Splatting [25], which proposed a differential rasterizer to render a large number of Gaussian ‘splats,’ each with their state including color, position, and covariance matrix. Gaussian splatting achieves real-time rendering of novel views with state-of-the-art performance.

### 2.2. Dynamic Novel View Synthesis

The assumption of static scenes in neural rendering approaches prevents application to real-world scenarios with moving objects and people, such as the dynamic and deformable scenes in this work. One line of work to address this assumption is adding a time dimension to NeRF modeling [15, 18, 27, 65], either condition the neural field on explicit time input or a time embedding. Another line of work learns a deformation field to map into a canonical space [41, 43], i.e., every 4D point in space and time maps to a 3D point in a canonical NeRF. This approach can be improved via distinguishing between foreground and back-

ground [52], or via leveraging depth priors [1, 37, 63], and can achieve fast training [16, 53].

To accelerate the training of dynamic neural radiance fields, DeVRF [30] proposed to model the 3D canonical space and 4D deformation field of a dynamic, non-rigid scene with explicit and discrete voxel-based representations. To solve the overfitting issue resulting from a large number of grid parameters, DeVRF [30] introduces a static-to-dynamic learning paradigm to first reconstruct a 3D canonical voxel space using static multi-view images and then optimize a 4D deformation voxel space using few-view dynamic sequences. It achieves convergence of optimizing dynamic voxel radiance fields within 10 minutes on a single NVIDIA GeForce RTX3090 GPU. However, since it relies on the static scene training stage to learn the scene information, it struggles to reconstruct dynamic scenes with complex deformations and shadows, especially with dynamic occlusions.

Several recent works extend the above approaches to 3D Gaussian splatting. Dynamic 3D Gaussians [33] explicitly model the position and covariance matrix of each Gaussian at each time step. This method struggles in dynamic scenes with large deformations, strong shadows, or occlusions. We build on another recent work, 4D Gaussian splatting [64], which uses feature encoding techniques proposed in Hex-Planes [6] and K-planes [17], and learns a deformation field instead. To the best of our knowledge, all prior deformation-based work learned deformations in a non-metric canonical space without reconstructing metric deformations. We propose a method to learn metric deformations from a set of Gaussians with canonical properties, deformed to metric space using a neural-voxel deformation function. By training on adjacent timesteps, MD-Splatting allows enforcing physics-informed regularization terms to improve performance beyond photometric consistency.

### 2.3. Point Tracking

Point tracking methods, usually trained on large amounts of data, aided previous 3D tracking approaches by providing a strong prior [30]. We also construct several baselines that include point tracking methods (Section 6). Prior work on point tracking often studies tracking 2D points across video frames, where a dominant approach is training models on large-scale synthetic datasets containing ground-truth point trajectories [13, 14, 22, 71] or dense optical flows [60]. Optical flow [3, 51] or scene flow [2, 56, 58] can also be viewed as single-step point-tracking in 2D and 3D, respectively.

Another relevant line of work tightly couples dynamic scene reconstruction and motion estimation of non-rigid objects. A predominant setup is fusing RGBD frames from videos of dynamic scenes or objects [38]. Tracking or correspondence-matching methods see a progression from template-based tracking of objects with known shape or

kinematics priors (such as human hand, face or body poses) [7, 40, 45], to more general shapes or scenes [4, 5, 72]. The main difference from these works is that we do not use depth input, and perform more rigorous quantitative evaluations on tracking specific points.

Most related to ours is the more recent methods that obtain tracking from neural scene rendering. DCT-NeRF[59] learns a coordinate-based neural scene representation that outputs continuous 3D trajectories across the whole input sequence. PREF [48] optimizes a dynamic space-time neural field with self-supervised motion prediction loss. Most recently, Luiten et al. [33] models dynamic 3D Gaussians explicitly across timestamps to achieve tracking. While our work also leverages 3D Gaussians, in contrary to the explicit modeling in Dynamic 3D Gaussians [33], we learn a deformation function that scales much better with video length, and we focus on deformable objects that are more challenging than the ball-throwing videos used in [33].

A main motivation for studying point tracking is the potential it can unlock for robotics applications: for example, RoboTAP [55] shows pre-trained point-tracking models improves sample efficiency of visual imitation learning.

## 3. Problem Statement

Given a set of timed image sequences captured from multiple cameras with known intrinsics and extrinsics, the objective is to learn a model that performs 3D tracking and novel view synthesis. Each image sequence is captured over the same time interval  $t \in [0, H]$ .

**3D Tracking** The 3D tracking objective is to recover the trajectory of any point in a dynamic scene by modeling metric deformations. Thus, the objective is to find a function  $x_t = Q(x_0, t_0, t)$ , where  $x_0 \in \mathbb{R}^3$  is the location of a point of interest at a chosen time  $t_0$ , while  $x_t \in \mathbb{R}^3$  is the location of the same point at another chosen time  $t$ . The function  $Q$  is valid for any point  $x_0$  and any  $t \in [0, H]$ , allowing for tracking of any point in space.

**Novel View Synthesis** This objective is to recover novel views from arbitrary viewpoints. The extrinsics at any view-point can be captured by matrix  $P$ , with  $P = K[R|T]$ . Here  $K$  is the intrinsics matrix,  $R$  is the rotation matrix of a camera with respect to the world frame, and  $T$  is the translation vector with respect to the world frame. The aim is to learn a function  $V$  such that  $I_{P,t} = V(P, t)$ , where  $I_{P,t}$  is an image rendered from a camera with extrinsics  $P$  at time  $t$ . As with the tracking objective, the time parameter is valid for any  $t \in [0, H]$ .

## 4. Preliminary

### 4.1. Neural Radiance Fields (NeRF)

Neural radiance fields (NeRFs) trace rays through multiple camera views to train an MLP  $\Phi_r$  to infer a radiance (RGB)

and density ( $\sigma$ ) from a world coordinate ( $x$ ) and view direction ( $\theta, \phi$ ) inputs, which are typically concatenated with a positional encoding in the form of sinusoids with varying frequencies.

$$\Phi_r(x, \theta, \phi) = (RGB\sigma) \quad (1)$$

## 4.2. Gaussian Splatting

3D Gaussian Splatting [25] deploys a more explicit scene representation than NeRFs, by rendering a large set of Gaussians each defined by their mean position  $\mu$  and covariance matrix  $\Sigma$ . Thus, for each  $x \in \mathbb{R}^3$ , its Gaussian  $G(x)$  is

$$G(x) = e^{-\frac{1}{2}(x-\mu)^T \Sigma^{-1}(x-\mu)},$$

Directly optimizing the covariance matrix  $\Sigma$  would lead to infeasible covariance matrices, as they have to be positive semi-definite to have a physical meaning. Instead, Gaussian Splatting [25] proposes to decompose  $\Sigma$  into a rotation  $R$  and scale  $S$  for each Gaussian:

$$\Sigma = RSS^T R^T,$$

and optimize  $R, S$ , and the mean position.

Given the transformation  $W$  of a camera, the covariance matrix can be projected into image space as

$$\Sigma' = JW\Sigma W^T J^T,$$

where  $J$  is the Jacobian of the affine approximation of the projective transformation.

During rendering, we compute the color  $C$  of a pixel by blending  $N$  ordered Gaussians overlapping the pixel :

$$C = \sum_{i \in N} c_i \alpha_i \prod_{j=1}^{i-1} (1 - \alpha_j).$$

where  $c_i$  is the color of each point and  $\alpha_i$  is given by evaluating a 2D Gaussian with covariance multiplied with a learned per-point opacity [25, 67].

## 4.3. Deformation Fields for Dynamic Scenes

Prior work showed that a deformation function combined with a static NeRF in a canonical space can enable novel view synthesis in dynamic scenes. The deformation function  $F_{\text{NeRF}} : \mathbb{R}^3 \rightarrow \mathbb{R}^3$  deforms a point in world coordinates ( $x'$ ) into a point in canonical space ( $x$ ). Prior work formulated  $F_{\text{NeRF}}$  as an MLP [42] and a multi-resolution voxel grid [16]. Wu et al. [64] applied a similar approach to arrive at Gaussian splatting of dynamic scenes. Given the state of a single canonical Gaussian, defined by  $P = [\mu, S, R, \sigma, C]$  at time  $t$ , a deformation function takes the form

$$P' = F_{4\text{DGS}}(P, t),$$

where  $F_{4\text{DGS}}$ , similar to the Hexplanes [6], contains a neural-voxel encoding in space and time. 4D-GS [64] starts with a *coarse* stage for initializing the canonical space, by setting  $P' = P$ , bypassing the deformation field and learning canonical properties directly. During the *fine* stage we learn the deformation function.

We propose MD-Splatting (Figure 2), based on 4D-Gaussians [64], to render novel views in dynamic scenes. The key differences with 4D-GS are: (1) we propose a simple method to track canonical Gaussians in 3D using a canonical  $\rightarrow$  metric deformation function, (2) the output of the deformation function is different, and (3) using the method shown in Figure 3, we enforce regularization losses on the 3D trajectories of Gaussians.

## 5. Method

MD-Splatting achieves high-quality novel view synthesis using a canonical space of Gaussians and a deformation function to deform them to metric space (Section 5.1). To incentivize learning physically plausible deformations, MD-Splatting introduces several regularization terms (Section 5.2).

### 5.1. 4D Gaussian Splatting

**Canonical Neural Voxel Encoding.** As with prior work, MD-Splatting learns a deformation function  $F$  from a canonical space. We use a neural-voxel encoding to ensure  $F$  has sufficient capacity to capture complex deformations. Prior work [16, 17, 36, 64] showed that neural-voxel encodings improve the speed and accuracy of novel view synthesis in dynamic scenes. We leverage HexPlanes [6, 64] to increase capacity for metric tracking and novel view synthesis simultaneously.

Figure 2 shows an overview of the canonical neural-voxel encoding. Each of the six voxel modules can be defined as  $R(i, j) \in \mathbb{R}^{h \times l N_i \times l N_j}$ . Here  $\{i, j\} \in \{(x, y), (x, z), (y, z), (x, t), (y, t), (z, t)\}$ , i.e., we adopt HexPlanes in all possible combinations.  $h$  is the size of each feature vector in the voxel,  $N_i, N_j$  are the sizes of the HexPlanes in each dimension,  $l$  is the upsampling scale. In every module, each plane has a different upsampling scale  $l$ . To query the multi-resolution voxel grids, we query each plane using bilinear interpolation to finally arrive at a feature vector used by the deformation MLP.

**Deformation MLP.** The deformation MLP takes in the voxel encoding and uses the encoding to deform the canonical Gaussians into metric space. Figure 2 shows the deformation MLP, which infers position, rotation, and a shadow scalar. We choose this set of outputs to model rigid-body transformations of each Gaussian and changes in illumination. Modeling changes in illumination is critical in the presence of shadows. The RGB color of each Gaussian is multiplied by the shadow scalar  $s \in [0, 1]$ , and the shadow

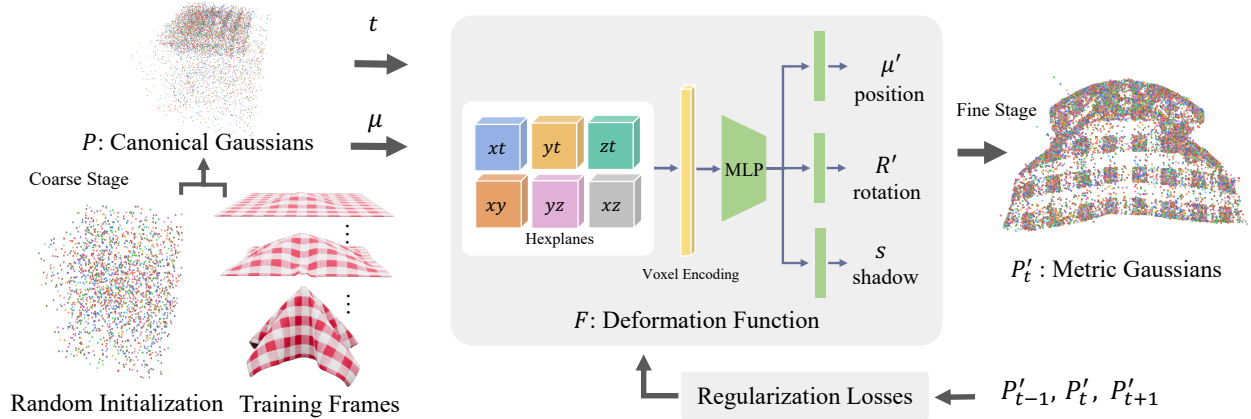


Figure 2. MD-Splatting maps a set of Gaussians with canonical properties to metric space using a deformation function  $F$ . The deformation function takes in the position of a Gaussian  $(x, y, z)$  and a queried timestamp  $t$ , to infer shadow  $s$ , rotation  $r'$  and metric position  $x'$ . During training, we use the metric positions and rotations to regularize the deformation function, considering the state at  $t = \{i - 1, i, i + 1\}$  with Gaussian metric states  $P'_{t-1}, P'_t, P'_{t+1}$

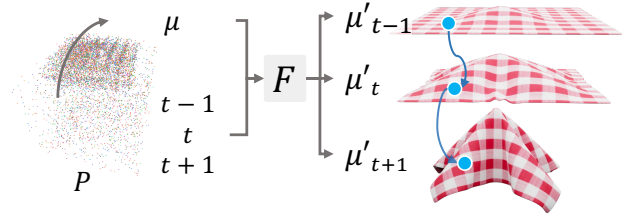


Figure 3. MD-Splatting uses three adjacent timesteps at every iteration to enforce physics-inspired regularization terms. All Gaussians are deformed to the metric space using the deformation function  $F$ , and rasterized to compute the photometric loss and its gradients. The positions of the Gaussians are used to compute the regularization terms based on local rigidity, isometry, and conservation of momentum (Section 5.2).

scalar is in the range  $[0, 1]$  by feeding the output of the MLP through a sigmoid activation function.

Next, we deform the Gaussians, modifying their mean positions  $\mu$ , rotation  $R$ , and color  $C$ , and arrive at a set of Gaussians in the metric space each with state  $P$ . The differentiable rasterizer from Gaussian Splatting [25] then renders the Gaussians to retrieve gradients for regressing both the canonical Gaussian states, and the parameters of the deformation function.

Unlike 4D-Gaussians [64], we propose to not infer opacity or scale using the deformation field. Optimizing for opacity and scale over time would allow Gaussians to disappear or appear instead of following the motion, which would make tracking less accurate. This design choice reduces the capacity of the deformation function, hence a lower view reconstruction quality as compared to 4D-Gaussians might be expected, see Table 2 for more information.

## 5.2. 3D Tracking using 4D Gaussians

**Motivation.** Figure 3 shows the process of tracking Gaussians from the canonical space in metric space. By querying the deformation function  $F$ , we can track the position of a Gaussian along the entire trajectory.

Without additional supervision, this approach will not necessarily converge to metric deformations. Especially when objects include areas with little texture and uniform color, the solution space for all metric deformations is underconstrained by photometric consistency supervision. To better learn a metric deformation, we propose regularization terms inspired by physics.

After empirically evaluating several combinations of regularization terms, we adopt the rigidity and isometry losses proposed in Luiten et al. and add a momentum term. The first two terms capture a local rigidity loss and local isometry loss, which we compute based on the state of the  $k$  nearest neighboring (KNN) Gaussians.

**Local Rigidity Loss** We assume the deformable material behaves linearly locally. With a large number of Gaussians, dense in 3D space, we expect nearest neighbors to move in similar directions and undergo similar rotations. Without this assumption, the trajectories of Gaussians are free to intersect and cross without a penalty. Instead, we introduce a local rigidity loss,

$$\mathcal{L}_{i,j,t}^{\text{rigid}} = w_{i,j} \| (\mu_{j,t-1} - \mu_{i,t-1}) - R_{i,t-1} R_{i,t}^{-1} (\mu_{j,t} - \mu_{i,t}) \|_2,$$

where  $\mu_{i,t}$  is the mean position of Gaussian  $i$  at time  $t$ ,  $R_{i,t}$  is the rotation matrix of Gaussian  $i$  at timestep  $t$ . This loss regularizes the change in position of the  $k$  nearest neighbors as seen from Gaussian  $i$ , by transforming the current offset of the neighbors to the previous Gaussian orientation. We

define

$$w_{i,j} = \exp(-\lambda_w \|\mu_{j,0} - \mu_{i,0}\|_2^2),$$

an isotropic Gaussian used to decrease the weight of Gaussians at a greater distance from  $\mu_{i,0}$ . When a sufficiently large  $\lambda_w$  is applied, and with a small enough  $k$  for KNN, this loss fits the local linearity assumption. The total rigidity loss at time  $t$  is

$$\mathcal{L}_t^{\text{rigid}} = \frac{1}{k|\mathcal{P}|} \sum_{i \in \mathcal{P}} \sum_{j \in \text{knn}_i} \mathcal{L}_{i,j,t}^{\text{rigid}}$$

Here  $\mathcal{P}$  is the set of all Gaussians.

**Local Isometry Loss** Another assumption we incentivize is to keep the relative position of the  $k$  nearest neighbors constant w.r.t.  $t = 0$ . With sufficient deformation, this assumption will be broken at a larger scale, but at a local scale, this regularization avoids drift from the ground truth trajectory. The isometry loss is

$$\mathcal{L}_t^{\text{iso}} = \frac{1}{k|\mathcal{P}|} \sum_{i \in \mathcal{P}} \sum_{j \in \text{knn}_i} w_{i,j} \|\mu_{j,0} - \mu_{i,0}\|_2 - \|\mu_{j,t} - \mu_{i,t}\|_2.$$

**Conservation of Momentum** The final term we add is to incentivize the conservation of momentum. Newton’s first law states objects without external forces applied, given some mass  $m$  and velocity vector  $\mathbf{v}$ , maintain their momentum  $m \cdot \mathbf{v}$ . We introduce the regularization term

$$\mathcal{L}_{i,t}^{\text{momentum}} = \|\mu_{i,t+1} + \mu_{i,t-1} - 2\mu_{i,t}\|_1.$$

This term incentivizes a constant velocity vector and has the effect of imposing a low-pass filter on the 3D trajectories. It smooths out trajectories with many sudden changes of direction and magnitude (momentum). Table 1 shows the impact of the proposed regularization terms on tracking errors.

## 6. Experiments

We test the effectiveness of MD-Splatting on synthetic datasets of deformable objects. Section 6.1 provides details on our experiment setup, evaluation metrics, and baseline methods. Section 6.2 reports evaluation results from the compared methods and result analysis. Section 6.3 supplies additional ablation results on the training efficiency of MD-Splatting.

### 6.1. Experiment Setup

**Dataset Preparation** We use Blender to model dynamic cloth sequences and render photo-realistic images. We create 6 distinct scenes, each containing a different cloth with distinct visual and physical properties, and we render images from 100 different camera views and 40 consecutive time steps for training for a total of 4,000 images. The

cloth deformations are introduced by dropping each cloth over one or a few invisible balls onto a ground plane or by constraining the cloth at an attachment point. We obtain ground-truth trajectories by tracking the mesh vertices of deformable objects in Blender.

**Baselines.** We compare to baseline methods: (1) 2D tracking approaches by projecting their inferences to 3D points using Blender’s ground truth depth and the camera’s ground truth projective geometry. While these methods were not designed for 3D tracking, they are well-known for their impressive 2D tracking performance. Their numbers aid in putting the tracking performance of the other baselines into context. We run RAFT [51] on all views and report the mean results as the RAFT model. We also provide two oracle methods which have access to privileged information: the ground truth trajectories. *RAFT Oracle* first evaluates on all views, to then output only the trajectories from the view with the lowest median trajectory error. We also report *OmniMotion Oracle*, which runs OmniMotion [60] on the frame with the lowest MTE for RAFT. Training OmniMotion takes roughly 12–13 hours on an Nvidia RTX 4090 GPU, making inference on all 100 views impractical. The numbers from *RAFT Oracle* and *OmniMotion Oracle* are not an apples-to-apples comparison with the other baselines, as to obtain their result they had to access privileged ground-truth trajectories.

(2) DeVRF [30] represents a dynamic, non-rigid scene with a 3D canonical voxel space and a 4D deformation voxel field. It proposes a 4D deformation cycle that models both the backward deformation from the deformed space to the canonical space and the forward deformation from the canonical space to the deformed space. Therefore, the point trajectories can be obtained by querying the forward deformation of canonical points at  $t = 0$  to every timestep’s deformed space through the 4D forward deformation space. While DeVRF was not designed for 3D tracking directly, it provides useful insight into how similar methods based on NeRF might perform in highly deformable scenes.

(3) Dynamic 3D Gaussians (*DynaGS*) [33], which also builds upon 3D Gaussian splatting for dynamic novel view synthesis, except it explicitly models the positions and rotations of each Gaussian at each time-step. This results in straightforward tracking of any point via finding the trajectory of the learned Gaussian with the highest influence on the given point. Although the original paper assumes a known point cloud at the first frame, we instead use a randomly sampled point cloud for a fair comparison, with *DynaGS* and MD-Splatting both not using depth information. We also ran with a point cloud initialized using ground-truth depth from Blender but saw very little to no improvement.

(4) Finally, we compare to tracking using 4D-Gaussians [64] (*4D-GS*). We add our approach for tracking canonical Gaussian, as shown in Figure 3, to extract 3D tra-

Metric	Method	Scene 1	Scene 2	Scene 3	Scene 4	Scene 5	Scene 6	Mean
3D MTE [mm] ↓	RAFT [51] <sup>a</sup>	89.687	151.363	295.66	135.468	125.554	67.861	144.266
	RAFT Oracle [51] <sup>a,b</sup>	27.328	34.629	104.842	24.976	32.331	36.113	43.370
	OmniMotion Oracle [60] <sup>a,b</sup>	16.188	<b>23.51</b>	92.536	11.064	57.603	19.624	36.754
	DeVRF [30]	147.293	78.487	449.74	123.745	77.736	133.391	168.399
	DynaGS [33]	17.189	54.409	<b>61.148</b>	19.870	24.081	26.757	33.909
	4D-GS [64]	7.788	93.409	118.692	16.422	7.033	4.600	41.324
	<b>MD-Splatting-NV</b> <b>MD-Splatting-TK</b>	5.173 <b>2.881</b>	63.894 <b>46.257</b>	81.917 88.169	<b>9.449</b> 9.686	5.679 <b>4.741</b>	3.385 <b>3.175</b>	28.250 <b>25.818</b>
3D $\delta_{\text{avg}}$ ↑	RAFT [51] <sup>a</sup>	0.442	0.229	0.128	0.295	0.395	0.434	0.321
	RAFT Oracle [51] <sup>a,b</sup>	0.623	0.562	0.247	0.651	0.573	0.509	0.528
	OmniMotion Oracle [60] <sup>a,b</sup>	0.763	<b>0.612</b>	0.301	0.763	0.448	0.680	0.595
	DeVRF [30]	0.344	0.368	0.094	0.326	0.471	0.398	0.334
	DynaGS [33]	0.774	0.401	0.317	0.697	0.649	0.607	0.574
	4D-GS [64]	0.787	0.337	0.257	0.700	0.817	0.883	0.630
	<b>MD-Splatting-NV</b> <b>MD-Splatting-TK</b>	0.851 <b>0.912</b>	0.428 <b>0.511</b>	0.346 <b>0.338</b>	0.749 <b>0.780</b>	0.870 <b>0.903</b>	0.919 <b>0.939</b>	0.694 <b>0.731</b>
3D Survival ↑	RAFT [51] <sup>a</sup>	0.935	0.891	0.738	0.919	0.807	0.891	0.864
	RAFT Oracle [51] <sup>a,b</sup>	<b>1.000</b>	<b>1.000</b>	<b>1.000</b>	<b>1.000</b>	0.999	0.974	0.996
	OmniMotion Oracle [60] <sup>a,b</sup>	<b>1.000</b>	0.993	<b>1.000</b>	0.991	0.870	<b>1.000</b>	0.976
	DeVRF [30]	<b>1.000</b>	0.972	0.571	0.952	0.860	0.862	0.870
	DynaGS [33]	<b>1.000</b>	<b>1.000</b>	0.958	<b>1.000</b>	<b>1.000</b>	<b>1.000</b>	0.993
	4D-GS [64]	<b>1.000</b>	0.978	0.967	<b>1.000</b>	0.999	<b>1.000</b>	0.991
	<b>MD-Splatting-NV</b> <b>MD-Splatting-TK</b>	0.999 <b>1.000</b>	<b>1.000</b> <b>1.000</b>	0.987 <b>1.000</b>	<b>1.000</b> <b>1.000</b>	<b>1.000</b> <b>1.000</b>	<b>1.000</b> <b>1.000</b>	0.998 <b>1.000</b>

<sup>a</sup> Method had access to ground truth depth. <sup>b</sup> Method had access to ground truth trajectories to pick the best camera view.

Table 1. 3D tracking results on the deformable cloth dataset (Figure 1). For each metric, the methods above the solid line had access to privileged information, see <sup>a,b</sup> and Section 6.1 for more details. The results suggest that MD-Splatting outperforms the baselines in all averaged metrics. DynaGS [33] and OmniMotion [60] are both competitive but accumulate large tracking errors in scenes 1, 5, and 6. The results also show the regularization parameters improve the tracking performance compared to 4D-GS [64].

jectories from a learning view synthesis model. Comparing to 4D-GS serves to show the impact of the changes made in the model architecture and the regularization terms, to arrive at MD-Splatting.

**Training and Evaluation Setup** We create a dataset of 6 dynamic cloth scenes, each with varying physical and visual properties. For MD-Splatting and 4D Gaussians, we follow [64] and perform 20,000 training iterations, and set point cloud pruning interval to 8,000, voxel plane resolution to [64, 64], and multi-resolution upsampling to levels  $L = \{1, 2, 4, 8\}$ . For Dynamic 3D Gaussians, we randomly sample the initial pointcloud with 10,000 points and use the same training hyperparameters as [33]. We set the regularization hyper parameters (Section 5.2) to  $\lambda_w = 100,000$ ,  $\lambda^{\text{rigid}} = 0.1$ ,  $\lambda^{\text{momentum}} = 0.1$ , and  $k = 5$  for KNN. We evaluate two parameters for  $\lambda^{\text{iso}}$  to better understand the impact of hyper parameters on 3D tracking and novel view synthesis. We evaluate MD-Splatting-NV with  $\lambda^{\text{iso}} = 0.01$ , and MD-Splatting-TK with  $\lambda^{\text{iso}} = 1.0$ . We ablate this parameter further in Section 6.4.

For DynaGS, we set  $\lambda^{\text{rigid}} = 4$ ,  $\lambda_w = 6,000$ ,  $\lambda^{\text{iso}} = 2.0$ , and  $k = 20$ , as in the open-source code. MD-Splatting enforces rigidity and isometry constraints only at a local scale.

We evaluate 3D tracking and novel-view synthesis re-

sults. For 3D tracking we evaluate each compared method on 1,000 randomly sampled points on each cloth. For novel-view synthesis, we evaluate using 200 unseen test-time cameras, and average the results across all cameras and all 40 time steps.

## 6.2. Main Results

**3D Point Tracking.** Following prior work [33, 71], we report median trajectory error (MTE), position accuracy ( $\delta$ ), and the survival rate with a threshold of 0.5 [m] [33].

The results are summarized in Table 1. We make the following observations: (1) MD-Splatting outperforms the baselines in all averaged metrics, with a 23.9% better average MTE compared to the baseline methods. Dynamic 3D Gaussians [33], OmniMotion [60], and RAFT [51] are competitive but accumulate a significantly larger tracking error in scenes 1, 4, 5, and 6. For example, in scene 1, the baselines have a MTE of at least 170% higher as compared to MD-Splatting. Excluding our implementation of 4D-GS [64] for tracking, the closest baseline is the OmniMotion [60] oracle model with a MTE 462% higher as compared to MD-Splatting. (2) MD-Splatting-TK performs better tracking compared to MD-Splatting NV, except for scene 3. The results suggest that setting  $\lambda^{\text{iso}} = 1.0$  leads to

Metrics	Method	Scene1	Scene2	Scene3	Scene 4	Scene5	Scene 6	Mean
PSNR $\uparrow$	DeVRF [30]	23.20	22.92	21.41	24.09	25.64	25.08	23.72
	DynaGS [33]	35.51	32.23	31.36	30.54	29.84	30.48	31.66
	4D-GS [64]	<b>40.76</b>	<b>40.14</b>	<b>44.38</b>	42.05	<b>33.70</b>	34.83	<b>39.31</b>
	<b>MD-Splatting-NV</b>	40.67	39.62	43.27	<b>42.61</b>	33.46	<b>34.96</b>	39.10
	<b>MD-Splatting-TK</b>	38.76	38.16	40.34	40.61	32.47	32.39	37.12
SSIM $\uparrow$	DeVRF [30]	0.87	0.92	0.96	0.97	0.89	0.85	0.91
	DynaGS [33]	0.96	0.93	0.95	0.96	0.92	0.95	0.94
	4D-GS [64]	<b>0.99</b>	<b>0.97</b>	<b>0.98</b>	<b>0.99</b>	<b>0.96</b>	<b>0.98</b>	<b>0.98</b>
	<b>MD-Splatting-NV</b>	<b>0.99</b>	<b>0.97</b>	<b>0.98</b>	<b>1.00</b>	<b>0.96</b>	<b>0.98</b>	<b>0.98</b>
	<b>MD-Splatting-TK</b>	<b>0.99</b>	<b>0.97</b>	<b>0.98</b>	<b>0.99</b>	0.95	0.97	<b>0.98</b>
LPIPS $\downarrow$	DeVRF [30]	0.13	0.16	0.18	0.14	0.16	0.18	0.16
	DynaGS [33]	0.03	0.11	0.16	0.07	0.10	0.06	0.09
	4D-GS [64]	<b>0.01</b>	<b>0.07</b>	<b>0.07</b>	<b>0.02</b>	<b>0.07</b>	<b>0.02</b>	<b>0.04</b>
	<b>MD-Splatting-NV</b>	<b>0.01</b>	<b>0.07</b>	<b>0.07</b>	<b>0.02</b>	0.08	<b>0.02</b>	0.05
	<b>MD-Splatting-TK</b>	0.02	0.08	0.08	0.03	0.08	0.04	0.05

Table 2. Novel view synthesis results on the deformable cloth dataset (Figure 1). The results suggest MD-Splatting significantly outperforms DynaGS [33] and DeVRF [30], while 4D-GS [64] performs slightly better. This is expected as a result of the additional regularization terms and deformation function design (Section 5). MD-Splatting only takes a minor decrease in view reconstruction performance, in order to significantly improve tracking. The results also suggest that MD-Splatting-TK performs worse in tracking as compared to MD-Splatting-NV, due to the stronger isometry regularization (Section 6.4).

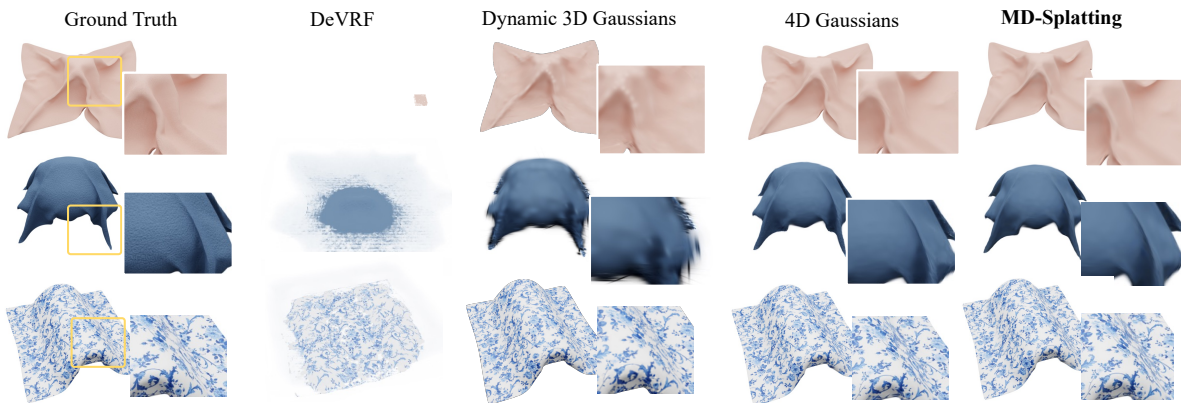


Figure 4. Qualitative novel view synthesis results from all baselines and MD-Splatting. Both 4D-GS [64] and MD-Splatting achieve the best qualitative results that are close to ground-truth renderings (especially on Scene 6, where the floral patterns on the cloth are reconstructed), albeit still fail to capture the fine-grained texture and wrinkles on Scene 2 and Scene3 cloth.

overall better tracking performance. Section 6.4 contains a more in-depth analysis on this parameter.

(3) MD-Splatting achieves the best performance in environments with textured cloth: scenes 1, 5, and 6. The texture makes photometric consistency a stronger supervision signal, leading to more accurate 3D tracking.

(4) The regularization parameters and change in deformation function architecture seem to improve the tracking performance compared to our implementation of 4D-GS [64]. MD-Splatting scores better metrics in all scenes. (5) The RAFT [51] and OmniMotion [60] results are highly dependent on the camera view angles, and we report the camera view with the best error values after evaluating all the test-time views; despite this given

advantage, these methods still fail to achieve consistent and competitive tracking performance.

We hypothesize that part of the tracking error from Dynamic 3D Gaussians [33] is a result of converging Gaussian states to local optima. Especially with larger deformations and shadows, we imagine Gaussians could converge to local optima with relatively large tracking errors. The other source of error we hypothesize plays a role is the various regularization terms and their hyperparameters, which are predominantly focused on rigid motion.

**Novel View Synthesis.** We evaluate visual reconstruction quality. In Table 2, we report results on the three standard metrics commonly used in prior work: PSNR [61],



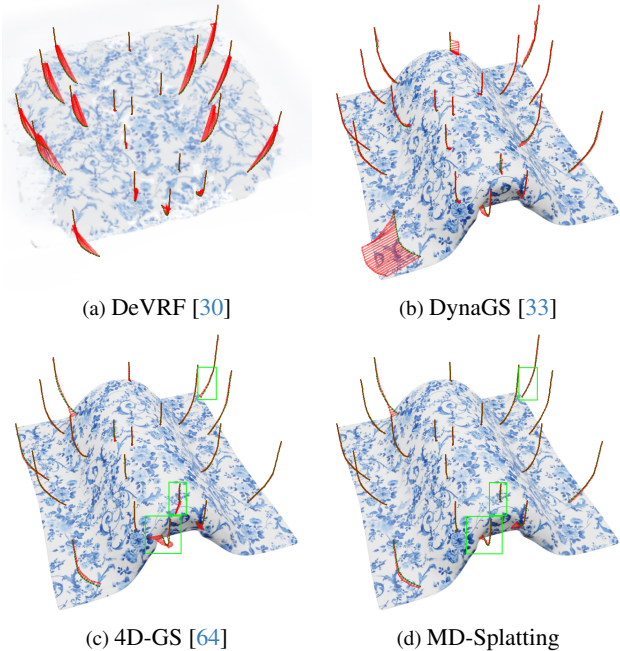


Figure 5. **Results on Scene 6:** randomly sampled ground-truth trajectories in green, inferred trajectories in red, and the error in red. The differences between 4D-GS [64] are marked with green squares. Compared to the baseline methods, MD-Splatting results in fewer errors in 3D tracking.

SSIM [62], and LPIPS [70]. MD-Splatting-NV performs comparably to 4D Gaussians (4D-GS) on SSIM while obtaining marginally lower results on PSNR and LPIPS. DynaGS performs worse on view synthesis by a considerable margin. DeVRF obtains the lowest performance, and it does worse on the Scene 2 and 3 as compared to the other scenes—this suggests the textureless cloths impose additional challenges that the model cannot capture. MD-Splatting-TK yields a lower quality view reconstruction as compared to MD-Splatting-NV, as a result of the stronger isometry regularization (Section 6.4).

We jointly analyze results from 3D tracking 1 and novel view synthesis 2. We observe that 4D-GS under-performs DynaGS at 3D tracking in median trajectory error, but out-performs DynaGS at novel view synthesis. MD-Splatting is designed to achieve the best of both worlds. While close to 4D-GS in nature, MD-Splatting can track deformations better than DynaGS while keeping the high-quality novel-view synthesis capability.

**Qualitative Results: Tracked Trajectories** Figure 5 shows a quantitative comparison for tracking performance in Scene 6, overlaid on each method’s renders. The randomly sampled trajectories show examples of trajectories where DeVRF [30] and Dynamic 3D Gaussians [33] diverge from the ground truth. For DeVRF [30], we hypothesize a lack of high-quality view reconstruction is the

Metric	Method	40 Steps	20 Steps	14 Steps	10 Steps
PSNR $\uparrow$	DynaGS [33]	29.99	14.15	13.734	14.05
	<b>MD-Splatting</b>	<b>33.47</b>	<b>33.00</b>	<b>32.80</b>	<b>32.91</b>
Training Time [mins] $\downarrow$	DynaGS [33]	94.96	81.71	71.43	61.30
	<b>MD-Splatting</b>	<b>35.68</b>	<b>21.12</b>	<b>20.21</b>	<b>23.76</b>
MTE [mm] $\downarrow$	DynaGS [33]	28.48	43.04	65.74	110.35
	<b>MD-Splatting</b>	<b>5.789</b>	<b>6.725</b>	<b>8.876</b>	<b>7.876</b>

Table 3. Ablation on the number of time steps provided for each camera view. Fewer time steps means a lower time resolution.

cause of poor tracking, whereas Dynamic 3D Gaussians [33] has high-quality view reconstruction but has a few trajectories diverge from the ground truth. The difference between 4D-GS and MD-Splatting-NV is more subtle, and can be observed in the areas marked with green boxes. The green boxes highlight areas where 4D-GS [64] struggles to maintain tracking, whereas MD-Splatting-NV achieves better tracking.

**Qualitative Results: Novel View Synthesis.** Figure 4 shows a qualitative comparison for scenes 2, 3, and 6. Both 4D-GS and MD-Splatting-NV achieve the best qualitative results that are close to ground-truth (notably on Scene 6, where the floral patterns on the cloth are reconstructed), albeit still fail to capture the fine-grained texture and wrinkles on Scene 2 and 3 cloth. DynaGS also achieves high-quality rendering overall but display a blurry visual effect around the deformed (i.e., wrinkled) areas. We hypothesize that regressing Gaussian positions and orientations is more unstable, and prone to converge to local optima. DeVRF nearly completely fails in Scene 3 due to the lack of textures: the model overfits to one small patch on the cloth and ignores the rest of the scene; it also shows difficulty in learning the large deformations on edges, i.e. only capturing colors around the center of the cloth.

### 6.3. Training Efficiency Ablation

We compare the training efficiency between MD-Splatting-NV and Dynamic 3D Gaussians [33] when decreasing the number of time steps provided from each camera view. We evaluate on Scene 5 and report PSNR on the subsampled frames, training time, and median trajectory error in Table 3. We observe that for MD-Splatting, training time is less affected by the number of frames from each camera view, as compared to Dynamic 3D Gaussians [33]. This is a result of its approach to train one time step at a time. The results also suggest that MD-Splatting has more robustness to larger deformations between frames, leading to a better PSNR and median trajectory error.

### 6.4. Isometry Loss Ablation

We ablate hyperparameter  $\mathcal{L}^{\text{iso}}$ , and show a trade-off between novel view synthesis and tracking (Figure 6). In this ablation, we compare PSNR $\uparrow$  and MTE [mm]  $\downarrow$ . We train

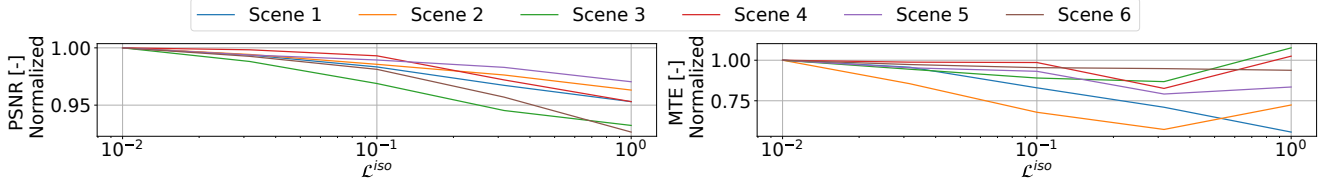


Figure 6. We ablate the  $\mathcal{L}^{\text{iso}}$  hyperparameter on the  $x$ -axis, and show the trade-off between novel view synthesis (left) and tracking (right). The left plot shows PSNR $\uparrow$  normalized for each Scene. The right plot shows median tracking error (MTE [mm]  $\downarrow$ ) normalized. The results suggest that a higher  $\mathcal{L}^{\text{iso}}$  leads to a lower PSNR, so worse view reconstruction quality due to more restrictions on the deformation function. A higher  $\mathcal{L}^{\text{iso}}$  leads to a lower MTE up to a point. Several scenes share a common local optima for MTE at  $\mathcal{L}^{\text{iso}} = 10^{-0.5}$ .

all scenes with 5 distinct hyperparameter values:  $\mathcal{L}^{\text{iso}} \in \{10^{-2}, 10^{-1.5}, 10^{-1}, 10^{-0.5}, 10^0\}$ , for a total of 30 experiments. The results suggest that a higher  $\mathcal{L}^{\text{iso}}$  leads to a lower PSNR, so worse view reconstruction quality due to more restrictions on the deformation function. A higher  $\mathcal{L}^{\text{iso}}$  also leads to a lower MTE up to  $\mathcal{L}^{\text{iso}} = 10^{-0.5}$ . We observe a common local optimum with the lowest MTE at  $\mathcal{L}^{\text{iso}} = 10^{-0.5}$  for several scenes. This points to potential directions for future research. Future research might explore improved parameter tuning techniques for all parameters, or even recover the parameters as part of the training process.

## 7. Conclusions

In this work, we address the challenging problem of simultaneous 3D point-tracking and novel view synthesis in dynamic scenes with highly deformable objects. We introduced MD-Splatting, the first approach that learns continuous metric deformations from a canonical space of Gaussians. We empirically demonstrate that MD-Splatting outperforms baseline methods and achieves both high-quality dynamic scene reconstruction and high-accuracy 3D tracking on highly deformed cloth objects with occlusions and shadows. We also contribute a dataset of six synthetic scenes to facilitate future research.

**Limitations and future work.** MD-Splatting, similar to prior work on dynamic novel view reconstruction, requires a setup of multiple synchronized and calibrated cameras, which may require a significant engineering effort in real-world scenarios. This work also focused on scenes with only a cloth as the visible object, more scenes, simulation or real, with soft objects in a larger environment would be helpful. These limitations point to promising directions for future research.

## References

- [1] Benjamin Attal, Eliot Laidlaw, Aaron Gokaslan, Changil Kim, Christian Richardt, James Tompkin, and Matthew O’Toole. Törf: Time-of-flight radiance fields for dynamic scene view synthesis. *Advances in Neural Information Processing Systems*, 34, 2021. 2, 3
- [2] Tali Basha, Yael Moses, and Nahum Kiryati. Multi-view scene flow estimation: A view centered variational approach. *International Journal of Computer Vision*, 101:6–21, 2010. 3
- [3] Steven S. Beauchemin and John L. Barron. The computation of optical flow. *ACM computing surveys (CSUR)*, 27(3):433–466, 1995. 3
- [4] Aljaž Božič, Michael Zollhöfer, Christian Theobalt, and Matthias Nießner. Deepdeform: Learning non-rigid rgb-d reconstruction with semi-supervised data, 2020. 3
- [5] Aljaž Božič, Pablo Palafox, Michael Zollhöfer, Angela Dai, Justus Thies, and Matthias Nießner. Neural non-rigid tracking, 2021. 3
- [6] Ang Cao and Justin Johnson. Hexplane: A fast representation for dynamic scenes. In *Proceedings of the IEEE/CVF Conference on Computer Vision and Pattern Recognition*, pages 130–141, 2023. 3, 4
- [7] Chen Cao, Yanlin Weng, Stephen Lin, and Kun Zhou. 3d shape regression for real-time facial animation. *ACM Transactions on Graphics (TOG)*, 32:1 – 10, 2013. 3
- [8] Lawrence Yunliang Chen, Huang Huang, Ellen Novoseller, Daniel Seita, Jeffrey Ichnowski, Michael Laskey, Richard Cheng, Thomas Kollar, and Ken Goldberg. Efficiently learning single-arm fling motions to smooth garments. In *Robotics Research*, pages 36–51, Cham, 2023. Springer Nature Switzerland. 1
- [9] Yue Chen, Xingyu Chen, Xuan Wang, Qi Zhang, Yu Guo, Ying Shan, and Fei Wang. Local-to-global registration for bundle-adjusting neural radiance fields. In *Proceedings of the IEEE/CVF Conference on Computer Vision and Pattern Recognition*, pages 8264–8273, 2023. 2
- [10] Julian Chibane, Aayush Bansal, Verica Lazova, and Gerard Pons-Moll. Stereo radiance fields (srf): Learning view synthesis from sparse views of novel scenes. In *IEEE Conference on Computer Vision and Pattern Recognition (CVPR)*, IEEE, 2021. 2
- [11] Blender Online Community. *Blender - a 3D modelling and*

- rendering package*. Blender Foundation, Stichting Blender Foundation, Amsterdam, 2018. 1
- [12] K. Deng, A. Liu, J. Zhu, and D. Ramanan. Depth-supervised nerf: Fewer views and faster training for free. In *2022 IEEE/CVF Conference on Computer Vision and Pattern Recognition (CVPR)*, pages 12872–12881, Los Alamitos, CA, USA, 2022. IEEE Computer Society. 2
- [13] Carl Doersch, Ankush Gupta, Larisa Markeeva, Adrià Recasens, Lucas Smaira, Yusuf Aytar, João Carreira, Andrew Zisserman, and Yi Yang. Tap-vid: A benchmark for tracking any point in a video. *Advances in Neural Information Processing Systems*, 35:13610–13626, 2022. 3
- [14] Carl Doersch, Yi Yang, Mel Vecerik, Dilara Gokay, Ankush Gupta, Yusuf Aytar, Joao Carreira, and Andrew Zisserman. Tapir: Tracking any point with per-frame initialization and temporal refinement. *arXiv preprint arXiv:2306.08637*, 2023. 3
- [15] Yilun Du, Yinan Zhang, Hong-Xing Yu, Joshua B. Tenenbaum, and Jiajun Wu. Neural radiance flow for 4d view synthesis and video processing. In *Proceedings of the IEEE/CVF International Conference on Computer Vision*, 2021. 2
- [16] Jiemin Fang, Taoran Yi, Xinggang Wang, Lingxi Xie, Xiopeng Zhang, Wenyu Liu, Matthias Nießner, and Qi Tian. Fast dynamic radiance fields with time-aware neural voxels. In *SIGGRAPH Asia 2022 Conference Papers*, 2022. 3, 4
- [17] Sara Fridovich-Keil, Giacomo Meanti, Frederik Rahbæk Warburg, Benjamin Recht, and Angjoo Kanazawa. K-planes: Explicit radiance fields in space, time, and appearance. In *Proceedings of the IEEE/CVF Conference on Computer Vision and Pattern Recognition*, pages 12479–12488, 2023. 3, 4
- [18] Chen Gao, Ayush Saraf, Johannes Kopf, and Jia-Bin Huang. Dynamic view synthesis from dynamic monocular video. In *Proceedings of the IEEE International Conference on Computer Vision*, 2021. 2
- [19] S. J. Garbin, M. Kowalski, M. Johnson, J. Shotton, and J. Valentin. Fastnerf: High-fidelity neural rendering at 200fps. In *2021 IEEE/CVF International Conference on Computer Vision (ICCV)*, pages 14326–14335, 2021. 2
- [20] Tuomas Haarnoja, Ben Moran, Guy Lever, Sandy H. Huang, Dhruva Tirumala, Markus Wulfmeier, Jan Humpalik, Saran Tunyasuvunakool, Noah Y. Siegel, Roland Hafner, Michael Bloesch, Kristian Hartikainen, Arunkumar Byravan, Leonard Hasenclever, Yuval Tassa, Fereshteh Sadeghi, Nathan Batchelor, Federico Casarini, Stefano Saliceti, Charles Game, Neil Sreendra, Kushal Patel, Marlon Gwira, Andrea Huber, Nicole Hurley, Francesco Nori, Raia Hadsell, and Nicolas Heess. Learning agile soccer skills for a bipedal robot with deep reinforcement learning, 2023. 1
- [21] Ayaan Haque, Matthew Tancik, Alexei Efros, Aleksander Holynski, and Angjoo Kanazawa. Instruct-nerf2nerf: Editing 3d scenes with instructions. In *Proceedings of the IEEE/CVF International Conference on Computer Vision*, 2023. 1
- [22] Adam W Harley, Zhaoyuan Fang, and Katerina Fragkiadaki. Particle video revisited: Tracking through occlusions using point trajectories. In *European Conference on Computer Vision*, pages 59–75. Springer, 2022. 3
- [23] Jeffrey Ichnowski\*, Yahav Avigal\*, Justin Kerr, and Ken Goldberg. Dex-NeRF: Using a neural radiance field to grasp transparent objects. In *Conference on Robot Learning (CoRL)*, 2020. 2
- [24] Yoonwoo Jeong, Seokjun Ahn, Christopher Choy, Anima Anandkumar, Minsu Cho, and Jaesik Park. Self-calibrating neural radiance fields. In *Proceedings of the IEEE/CVF International Conference on Computer Vision (ICCV)*, pages 5846–5854, 2021. 2
- [25] Bernhard Kerbl, Georgios Kopanas, Thomas Leimkühler, and George Drettakis. 3d gaussian splatting for real-time radiance field rendering. *ACM Transactions on Graphics*, 42(4), 2023. 2, 4, 5
- [26] Justin Kerr, Letian Fu, Huang Huang, Yahav Avigal, Matthew Tancik, Jeffrey Ichnowski, Angjoo Kanazawa, and Ken Goldberg. Evo-nerf: Evolving nerf for sequential robot grasping of transparent objects. In *Proceedings of The 6th Conference on Robot Learning*, pages 353–367. PMLR, 2023. 2
- [27] Z. Li, S. Niklaus, N. Snavely, and O. Wang. Neural scene flow fields for space-time view synthesis of dynamic scenes. In *2021 IEEE/CVF Conference on Computer Vision and Pattern Recognition (CVPR)*, pages 6494–6504, Los Alamitos, CA, USA, 2021. IEEE Computer Society. 2
- [28] Vincent Lim, Huang Huang, Lawrence Yunliang Chen, Jonathan Wang, Jeffrey Ichnowski, Daniel Seita, Michael Laskey, and Ken Goldberg. Real2sim2real: Self-supervised learning of physical single-step dynamic actions for planar robot casting. In *2022 International Conference on Robotics and Automation (ICRA)*, pages 8282–8289, 2022. 1
- [29] Chen-Hsuan Lin, Wei-Chiu Ma, Antonio Torralba, and Simon Lucey. Barf: Bundle-adjusting neural radiance fields. In *IEEE International Conference on Computer Vision (ICCV)*, 2021. 2
- [30] Jia-Wei Liu, Yan-Pei Cao, Weijia Mao, Wenqiao Zhang, David Junhao Zhang, Jussi Keppo, Ying Shan, Xiaohu Qie, and Mike Zheng Shou. Devrf: Fast deformable voxel radiance fields for dynamic scenes. *Advances in Neural Information Processing Systems*, 35:36762–36775, 2022. 3, 6, 7, 8, 9
- [31] Lingjie Liu, Jiatao Gu, Kyaw Zaw Lin, Tat-Seng Chua, and Christian Theobalt. Neural sparse voxel fields. *NeurIPS*, 2020. 2
- [32] Stephen Lombardi, Tomas Simon, Gabriel Schwartz, Michael Zollhoefer, Yaser Sheikh, and Jason Saragih. Mixture of volumetric primitives for efficient neural rendering. *ACM Trans. Graph.*, 40(4), 2021. 2
- [33] Jonathon Luiten, Georgios Kopanas, Bastian Leibe, and Deva Ramanan. Dynamic 3d gaussians: Tracking by persistent dynamic view synthesis. *arXiv preprint arXiv:2308.09713*, 2023. 2, 3, 5, 6, 7, 8, 9
- [34] Ben Mildenhall, Pratul P. Srinivasan, Matthew Tancik, Jonathan T. Barron, Ravi Ramamoorthi, and Ren Ng. Nerf: Representing scenes as neural radiance fields for view synthesis. In *ECCV*, 2020. 2

- [35] Muhammad Husnain Mubarak, Ramakrishna Kanungo, Tobias Zirr, and Rakesh Kumar. Hardware acceleration of neural graphics, 2023. [2](#)
- [36] Thomas Müller, Alex Evans, Christoph Schied, and Alexander Keller. Instant neural graphics primitives with a multi-resolution hash encoding. *ACM Trans. Graph.*, 41(4):102:1–102:15, 2022. [2](#), [4](#)
- [37] Thomas Neff, Pascal Stadlbauer, Mathias Parger, Andreas Kurz, Joerg H. Mueller, Chakravarty R. Alla Chaitanya, Anton S. Kaplanyan, and Markus Steinberger. DONeRF: Towards Real-Time Rendering of Compact Neural Radiance Fields using Depth Oracle Networks. *Computer Graphics Forum*, 40(4), 2021. [2](#), [3](#)
- [38] Richard A. Newcombe, Dieter Fox, and Steven M. Seitz. Dynamicfusion: Reconstruction and tracking of non-rigid scenes in real-time. In *2015 IEEE Conference on Computer Vision and Pattern Recognition (CVPR)*, pages 343–352, 2015. [3](#)
- [39] Michael Niemeyer, Jonathan T. Barron, Ben Mildenhall, Mehdi S. M. Sajjadi, Andreas Geiger, and Noha Radwan. Regnerf: Regularizing neural radiance fields for view synthesis from sparse inputs. In *Proc. IEEE Conf. on Computer Vision and Pattern Recognition (CVPR)*, 2022. [2](#)
- [40] Iasonas Oikonomidis, Nikolaos Kyriazis, and Antonis A. Argyros. Efficient model-based 3d tracking of hand articulations using kinect. In *British Machine Vision Conference*, 2011. [3](#)
- [41] Keunhong Park, Utkarsh Sinha, Jonathan T. Barron, Sofien Bouaziz, Dan B Goldman, Steven M. Seitz, and Ricardo Martin-Brualla. Nerfies: Deformable neural radiance fields. *ICCV*, 2021. [2](#)
- [42] Albert Pumarola, Enric Corona, Gerard Pons-Moll, and Francesc Moreno-Noguer. D-nerf: Neural radiance fields for dynamic scenes. In *Proceedings of the IEEE/CVF Conference on Computer Vision and Pattern Recognition*, pages 10318–10327, 2021. [2](#), [4](#)
- [43] Albert Pumarola, Enric Corona, Gerard Pons-Moll, and Francesc Moreno-Noguer. D-NeRF: Neural Radiance Fields for Dynamic Scenes. In *Proceedings of the IEEE/CVF Conference on Computer Vision and Pattern Recognition*, 2021. [2](#)
- [44] Christian Reiser, Songyou Peng, Yiyi Liao, and Andreas Geiger. Kilonerf: Speeding up neural radiance fields with thousands of tiny mlps. *CoRR*, abs/2103.13744, 2021. [2](#)
- [45] Tanner Schmidt, Richard A. Newcombe, and Dieter Fox. Dart: dense articulated real-time tracking with consumer depth cameras. *Autonomous Robots*, 39:239 – 258, 2015. [3](#)
- [46] Daniel Seita, Aditya Ganapathi, Ryan Hoque, Minh Hwang, Edward Cen, Ajay Kumar Tanwani, Ashwin Balakrishna, Brijen Thananjeyan, Jeffrey Ichnowski, Nawid Jamali, Katsu Yamane, Soshi Iba, John Canny, and Ken Goldberg. Deep Imitation Learning of Sequential Fabric Smoothing From an Algorithmic Supervisor. In *IEEE/RSJ International Conference on Intelligent Robots and Systems (IROS)*, 2020. [1](#)
- [47] Kaushik Shivakumar, Vainavi Viswanath, Anrui Gu, Yahav Avigal, Justin Kerr, Jeffrey Ichnowski, Richard Cheng, Thomas Kollar, and Ken Goldberg. Sgfm 2.0: Autonomously untangling long cables using interactive perception. In *2023 IEEE International Conference on Robotics and Automation (ICRA)*, pages 5837–5843, 2023. [1](#)
- [48] Liangchen Song, Xuan Gong, Benjamin Planche, Meng Zheng, David Doermann, Junsong Yuan, Terrence Chen, and Ziyang Wu. Pref: Predictability regularized neural motion fields. In *European Conference on Computer Vision*, 2022. [3](#)
- [49] Edgar Sucar, Shikun Liu, Joseph Ortiz, and Andrew Davison. iMAP: Implicit mapping and positioning in real-time. In *Proceedings of the International Conference on Computer Vision (ICCV)*, 2021. [2](#)
- [50] Cheng Sun, Min Sun, and Hwann-Tzong Chen. Direct voxel grid optimization: Super-fast convergence for radiance fields reconstruction. In *CVPR*, 2022. [2](#)
- [51] Zachary Teed and Jia Deng. Raft: Recurrent all-pairs field transforms for optical flow. In *Computer Vision—ECCV 2020: 16th European Conference, Glasgow, UK, August 23–28, 2020, Proceedings, Part II 16*, pages 402–419. Springer, 2020. [3](#), [6](#), [7](#), [8](#)
- [52] Edgar Tretschk, Ayush Tewari, Vladislav Golyanik, Michael Zollhöfer, Christoph Lassner, and Christian Theobalt. Non-rigid neural radiance fields: Reconstruction and novel view synthesis of a deforming scene from monocular video, 2020. [3](#)
- [53] Edgar Tretschk, Ayush Tewari, Vladislav Golyanik, Michael Zollhöfer, Christoph Lassner, and Christian Theobalt. Non-rigid neural radiance fields: Reconstruction and novel view synthesis of a dynamic scene from monocular video. In *IEEE International Conference on Computer Vision (ICCV)*. IEEE, 2021. [3](#)
- [54] Prune Truong, Marie-Julie Rakotosaona, Fabian Manhardt, and Federico Tombari. Sparf: Neural radiance fields from sparse and noisy poses. *IEEE/CVF Conference on Computer Vision and Pattern Recognition, CVPR*, 2023. [2](#)
- [55] Mel Vecerik, Carl Doersch, Yi Yang, Todor Davchev, Yusuf Aytar, Guangyao Zhou, Raia Hadsell, Lourdes Agapito, and Jon Scholz. Robotap: Tracking arbitrary points for few-shot visual imitation. *arXiv preprint arXiv:2308.15975*, 2023. [3](#)
- [56] Sundar Vedula, Simon Baker, Peter Rander, Robert Collins, and Takeo Kanade. Three-dimensional scene flow. In *Proceedings of the Seventh IEEE International Conference on Computer Vision*, pages 722–729. IEEE, 1999. [3](#)
- [57] Dor Verbin, Peter Hedman, Ben Mildenhall, Todd Zickler, Jonathan T. Barron, and Pratul P. Srinivasan. Ref-NeRF: Structured view-dependent appearance for neural radiance fields. *CVPR*, 2022. [2](#)
- [58] Christoph Vogel, Konrad Schindler, and Stefan Roth. 3d scene flow estimation with a piecewise rigid scene model. *International Journal of Computer Vision*, 115:1–28, 2015. [3](#)
- [59] Chaoyang Wang, Ben Eckart, Simon Lucey, and Orazio Gallo. Neural trajectory fields for dynamic novel view synthesis, 2021. [3](#)
- [60] Qianqian Wang, Yen-Yu Chang, Ruojin Cai, Zhengqi Li, Bharath Hariharan, Aleksander Holynski, and Noah Snavely.

- Tracking everything everywhere all at once. In *International Conference on Computer Vision*, 2023. 3, 6, 7, 8
- [61] Zhou Wang, Alan C Bovik, Hamid R Sheikh, and Eero P Simoncelli. Image quality assessment: from error visibility to structural similarity. *TIP*, 2004. 8
- [62] Zhou Wang, Alan C Bovik, Hamid R Sheikh, and Eero P Simoncelli. Image quality assessment: from error visibility to structural similarity. *TIP*, 2004. 9
- [63] Yi Wei, Shaohui Liu, Yongming Rao, Wang Zhao, Jiwen Lu, and Jie Zhou. Nerfingmvs: Guided optimization of neural radiance fields for indoor multi-view stereo. In *ICCV*, 2021. 2, 3
- [64] Guanjun Wu, Taoran Yi, Jiemin Fang, Lingxi Xie, Xiaopeng Zhang, Wei Wei, Wenyu Liu, Qi Tian, and Xinggang Wang. 4d gaussian splatting for real-time dynamic scene rendering. *arXiv preprint arXiv:2310.08528*, 2023. 3, 4, 5, 6, 7, 8, 9
- [65] W. Xian, J. Huang, J. Kopf, and C. Kim. Space-time neural irradiance fields for free-viewpoint video. In *2021 IEEE/CVF Conference on Computer Vision and Pattern Recognition (CVPR)*, pages 9416–9426, Los Alamitos, CA, USA, 2021. IEEE Computer Society. 2
- [66] Lin Yen-Chen, Pete Florence, Jonathan T. Barron, Alberto Rodriguez, Phillip Isola, and Tsung-Yi Lin. iNeRF: Inverting neural radiance fields for pose estimation. In *IEEE/RSJ International Conference on Intelligent Robots and Systems (IROS)*, 2021. 2
- [67] Wang Yifan, Felice Serena, Shihao Wu, Cengiz Öztireli, and Olga Sorkine-Hornung. Differentiable surface splatting for point-based geometry processing. *ACM Transactions on Graphics*, 38(6):1–14, 2019. 4
- [68] Alex Yu, Ruilong Li, Matthew Tancik, Hao Li, Ren Ng, and Angjoo Kanazawa. PlenOctrees for real-time rendering of neural radiance fields. In *ICCV*, 2021. 2
- [69] Jason Y. Zhang, Gengshan Yang, Shubham Tulsiani, and Deva Ramanan. NeRS: Neural reflectance surfaces for sparse-view 3d reconstruction in the wild. In *Conference on Neural Information Processing Systems*, 2021. 2
- [70] Richard Zhang, Phillip Isola, Alexei A Efros, Eli Shechtman, and Oliver Wang. The unreasonable effectiveness of deep features as a perceptual metric. In *Proceedings of the IEEE conference on computer vision and pattern recognition*, pages 586–595, 2018. 9
- [71] Yang Zheng, Adam W Harley, Bokui Shen, Gordon Wetstein, and Leonidas J Guibas. Pointodyssey: A large-scale synthetic dataset for long-term point tracking. In *Proceedings of the IEEE/CVF International Conference on Computer Vision*, pages 19855–19865, 2023. 3, 7
- [72] Michael Zollhöfer, Matthias Nießner, Shahram Izadi, Christoph Rhemann, Christopher Zach, Matthew Fisher, Chenglei Wu, Andrew William Fitzgibbon, Charles T. Loop, Christian Theobalt, and Marc Stamminger. Real-time non-rigid reconstruction using an rgb-d camera. *ACM Transactions on Graphics (TOG)*, 33:1 – 12, 2014. 3